Dilute Aqueous-Aprotic Hybrid Electrolyte Enabling A Wide Electrochemical Window through Solvation Structure Engineering

Shuilin Wu, Bizhe Su, Mingzi Sun, Kaili Zhang, Denis Y. W. Yu, Bolong Huang*, Pengfei Wang, Chun-Sing Lee, Wenjun Zhang*

Dr. Shuilin Wu, Prof. Chun-Sing Lee, Prof. Wenjun Zhang

Department of Materials Science and Engineering, & Center of Super-Diamond and Advanced Films, City University of Hong Kong, 83 Tat Chee Avenue, Hong Kong, China

E-mail: apwjzh@cityu.edu.hk

Dr. Bizhe Su, Dr. Denis Y. W. Yu

School of Energy and Environment, City University of Hong Kong, 83 Tat Chee Avenue, Hong Kong, China

Prof. Kaili Zhang

Department of Mechanical Engineering, City University of Hong Kong, 83 Tat Chee Avenue, Hong Kong, China

Mingzi Sun, Prof. Bolong Huang,

Department of Applied Biology and Chemical Technology, The Hong Kong Polytechnic University, Hung Hom, Kowloon, Hong Kong, China

Email: bhuang@polyu.edu.hk

Prof. Pengfei Wang

Key Laboratory of Photochemical Conversion and Optoelectronic Materials and CityU-CAS Joint Laboratory of Functional Materials and Devices, Technical Institute of Physics and Chemistry, Chinese Academy of Sciences, Beijing 100190, P.R. China

Abstract

The application of super-concentrated aqueous electrolytes has shown great potentials in developing high-voltage electrochemical double-layer capacitors (EDLCs). However, the broadening of electrochemical windows of such super-concentrated electrolytes is at the expense of their high cost, low ionic conductivity, high density, and narrow operating temperature range.[1] Herein, we demonstrate a facile approach to expand the electrochemical window by regulating the solvation structure of the electrolyte through the introduction of trimethyl phosphate (TMP). Such an electrolyte successfully suppresses the decomposition of water, leading to a broad electrochemical window of 3 V even at low salt concentrations (*e.g.*, 3 m $NaClO_4$). Based on the dilute hybrid electrolyte, the EDLCs constructed by using porous graphene electrodes is able to operate within an enlarged voltage window of 0-2.4 V at a wide range of temperatures from -20 to 60 ºC. Moreover, the EDLCs also present excellent rate capability and cycle stability, *i.e.*, 83% capacitance retention after 100, 000 cycles. Density functional theory (DFT) calculations verify that TMP induces a significant electronic modulation for the bonding environment of the electrolyte, which enables the stronger binding of Na^+-H_2O with freely migrating TMP to expand the voltage window to exceed the potential limitation of aqueous electrolytes. This work has opened up a new direction for designing the advanced and efficient EDLCs in the future.

Introduction

Electrochemical double-layer capacitors (EDLCs) are promising energy storage devices for applications that require high power output and a long lifespan.[2] In commercial EDLCs, organic electrolytes have been widely used because of their broad electrochemical windows which enable a high operation voltage and thereof an increased energy density.[3]

Nevertheless, the flammability, volatility, and toxicity of organic electrolytes bring in safety concerns.[4] Moreover, the critical requirement on the high purity of organic electrolytes inevitably increases the cost of EDLCs.[5] Using low-cost and inherently safe aqueous-based electrolytes is a promising approach to fundamentally tackle the above problems. However, the narrow electrochemical window of water molecules (~1.23 V) limits the energy density of EDLCs which is proportional to the square of operation voltage.[6]

By dissolving a high concentration of salts in water (namely water-in-salt electrolytes with salt/solvent ratio > 1 by volume or weight), most of the water molecules are solvated with the cations and/or anions, and thus the decomposition of water molecules is suppressed, which efficiently expands the electrochemical windows of the aqueous electrolytes (usually >2.4 V). Thus far, various super-concentrated electrolytes have been developed based on fluorine-containing salts of high solubility.[7] Despite the substantially broadened electrochemical windows of these electrolytes, the use of concentrated fluorine-containing salts brings in cost and toxicity issues which are concerns for practical applications. Alternatively, some low-cost fluorine-free salts (such as sodium perchlorate ($NaClO_4$), and acetate salts (LiAc and KAc))[8] and small molecules (*e.g.*, urea and sugar)[9] can also broaden the electrochemical windows of the electrolytes with ultra-high concentrations. However, the problems with respect to the low ionic conductivity, high viscosity, and poor wettability of the super-concentrated electrolytes, which compromise the rate capability of EDLCs, are still unresolved.[10] Besides, the variation of salt solubility upon temperature limits the operation temperature range of such super-concentrated electrolytes; and the use of highly concentrated salts in electrolytes inevitably increases the electrolyte density and brings in extra weight, which leads to a decreased energy density at the device level. Therefore, low-cost dilute aqueous-based electrolytes with a wide electrochemical window are highly desirable. Recently, Lu and co-workers reported a dilute electrolyte of 2 m LiTFSI in a mixture of 6

w.t. % water and 94 w.t.% PEG (poly(ethylene glycol), which delivered an electrochemical window of 3.2 V benefiting from the reduced water decomposition under the strong hydrogen bonds between water and PEG molecules.[11] However, the high viscosity of PEG leads to a low ionic conductivity of such electrolyte (0.8 mS cm^{-1}) which is detrimental to achieving a high rate capability of EDLCs.

In this work, we report a dilute hybrid electrolyte, *i.e.*, 3 m $NaClO_4$ (*m* denoting molar per kilogram solvent) in a mixture of water and trimethyl phosphate (TMP), which is featured with a comparable electrochemical window to that of super-concentrated electrolytes. The $NaClO_4$ was selected as the salt for the hybrid electrolyte because of its low cost, earth abundance, and high solubility both in water and TMP. As verified by the density functional theory (DFT) simulations, the bonding energy between TMP and Na cations is much lower than that between water molecules and Na cations. Thus, the water molecules are strongly constrained around the Na cations, and the solvated structures are isolated by the free TMP molecules in the hybrid electrolyte. As a result, the decomposition of water is substantially restrained to guarantee a wide electrochemical window (2.9-3.2 V) even in a dilute hybrid electrolyte. Meanwhile, the hybrid electrolyte also demonstrates high ionic conductivity (23 mS cm^{-1}), low density (1.37 g cm^{-3}), and wide temperature compatibility. Significantly, the EDLCs based on the hybrid electrolyte not only operate within a wide voltage (0-2.4 V) and temperature range (-20 to 60 ºC) but also presents excellent rate capability and cycle stability (e.g., 83% capacitance retention after 100, 000 cycle at 25 ºC). This work will supply significant references in achieving highly desirable electrolyte for EDLCs through an cheap and efficient method.

Results and discussion

The hybrid electrolytes were obtained by diluting the super-concentrated 18 m $NaClO_4$ aqueous electrolytes with TMP to certain concentrations (e.g., 1 m, 3 m, and 6 m). Specifically, the mass ratio of $NaClO_4$, water, and TMP in the 1 m, 3 m, and 6 m hybrid electrolytes are 11:5:85, 11:5:25, and 11:5:10, respectively. The electrochemical windows of the hybrid electrolytes were evaluated by linear sweep voltammetry (LSV) based on a three-electrode system at a scan rate of 10 mV s^{-1}. For the measurements, Pt, silver chloride (Ag/AgCl), and carbon cloth were used as the working, reference, and counter electrodes, respectively. The 1 m and 18 m $NaClO_4$ aqueous electrolytes were also tested for reference.

As shown in Figure 1a-c, the electrochemical windows of these electrolytes are affected by the electrochemical stability of water, in which the hydrogen evolution and oxygen evolution reactions of water confine the lower and upper potential limits of the electrolyte, respectively. Significantly, it is revealed that the hybrid electrolytes demonstrate expanded electrochemical windows (2.9~3.2 V) in comparison with the dilute 1 m $NaClO_4$ aqueous electrolyte (2.4 V) and even the super-concentrated 18 m $NaClO_4$ aqueous electrolyte (2.9 V). Compared with the dilute 1 m $NaClO_4$ aqueous electrolyte, the much broadened electrochemical window of the 1 m hybrid electrolytes indicates that the addition of TMP can indeed restrain the decomposition of water even at a diluted concentration of salt. The hybrid electrolytes show slightly decreased electrochemical windows albeit with the increased concentration of salts, *i.e.*, 3.2 V, 3.0 V, and 2.9 V for 1 m, 3 m, and 6 m hybrid electrolytes, respectively (Figure 1d).

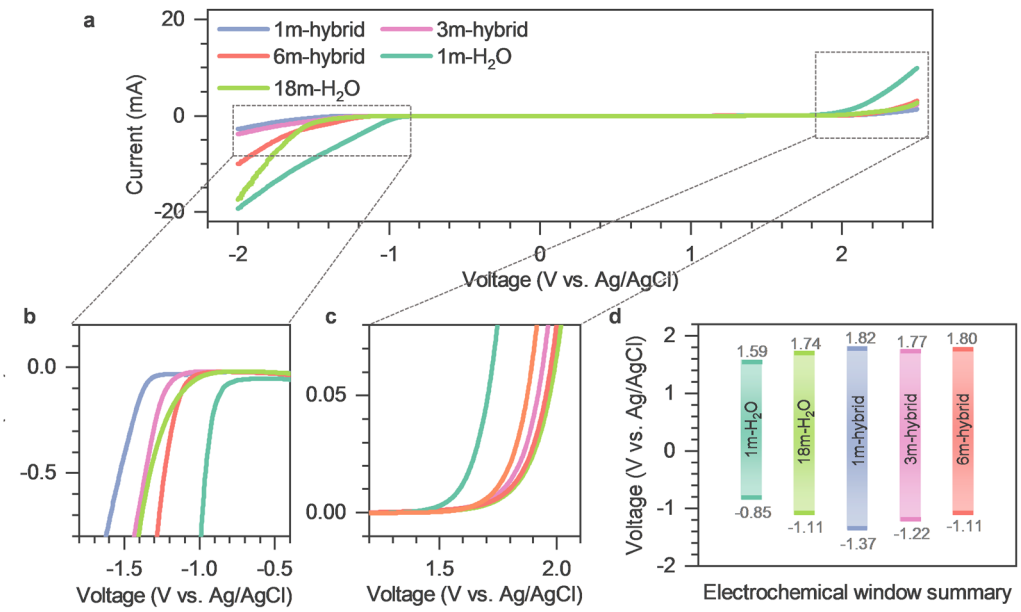

Figure 1. Electrochemical stability windows of hybrid electrolytes with various $NaClO_4$ concentrations. (a) LSV curves measured at a scan rate of 10 mV s^{-1} in a three-electrode system. The 1 m and 18 m $NaClO_4$ aqueous electrolytes without the addition of TMP were also tested for reference. (b) and (c) The enlarged views of the regions corresponding to the potentials for hydrogen and oxygen evolutions, respectively. (d) Bar charts of the electrochemical windows of hybrid and aqueous electrolytes.

The electrochemical performance of the EDLCs with different hybrid electrolytes was evaluated based on a symmetric cell configuration using the chemically activated microwave exfoliated graphene oxide (aMEGO, Figure S1, supporting information) electrodes. In the galvanostatic charge-discharge and cyclic voltammetry tests within the voltage range of 0-2.4 V, the cells with hybrid electrolytes show linear and symmetric charge-discharge curves at 0.5 A g^{-1} (Figure 2a), and quasi-rectangular cyclic voltammetry curves with a scan rate of 10 mV s^{-1} (Figure 2b), implying that the hybrid electrolytes enable the EDLCs with a stable operation voltage up to 2.4 V. With the further increased cut-off voltage to 2.6 V (Figure S2a and S2b, supporting information), the charge-discharge curves are still linear and symmetric in 1 m and 3 m hybrid electrolytes. However, a slightly decreased Coulombic efficiency is

observed. Moreover, the EDLCs with 1 m and 18 m aqueous electrolytes were also tested for comparison (Figure 2a, 2b, S3 and S4, supporting information). In sharp contrast, the 1 m and 18 m aqueous electrolytes can only be stably cycled below 2.0 V and 2.2 V, respectively. Such results indicate that the hybrid electrolytes can increase the operating voltages of the EDLCs by 1.2 and 1.1 times, and thus promote the energy density by 1.44 and 1.21 times as compared to the EDLCs with the 1 m and 18 m aqueous electrolytes.

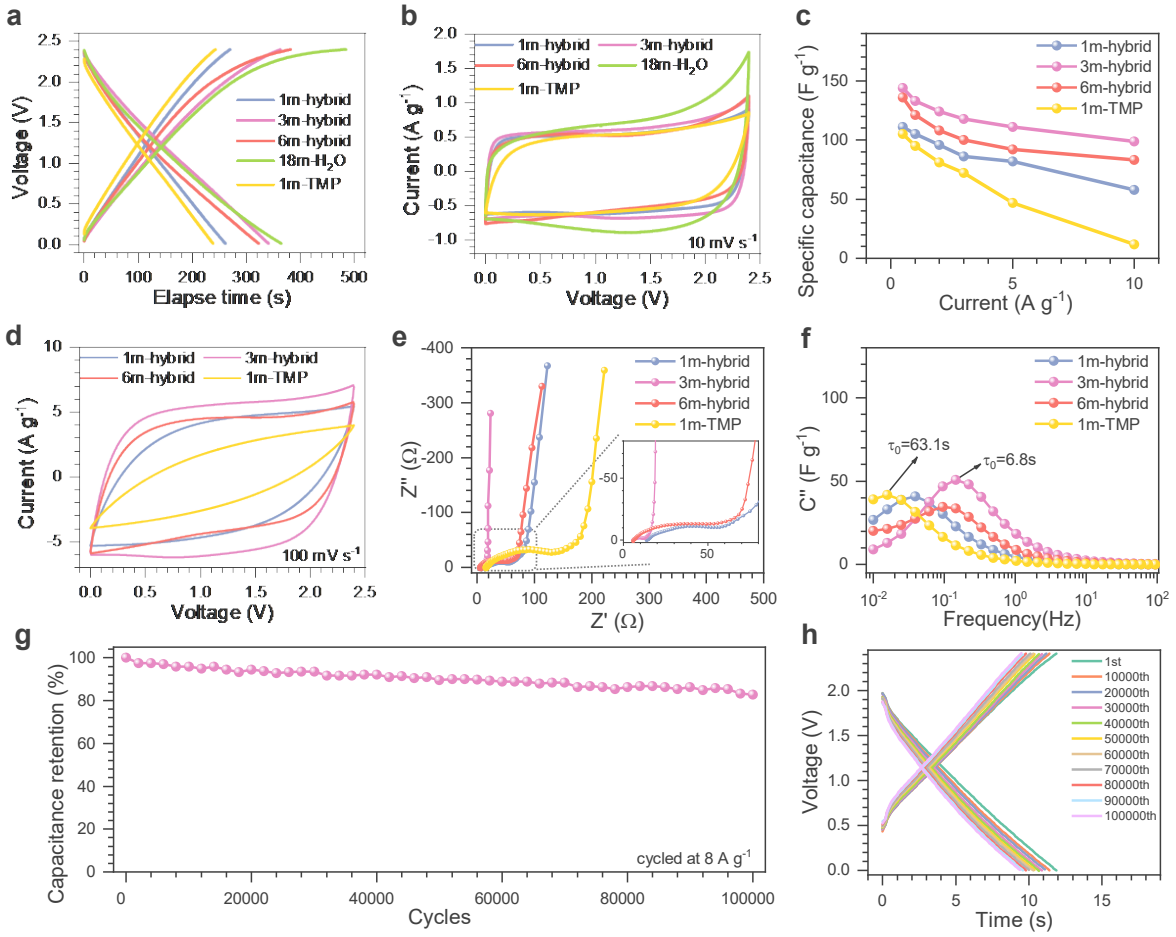

Figure 2. Electrochemical performance of the aMEGO-based EDLCs in hybrid electrolytes at 25 °C. (a) Galvanostatic charge-discharge curves of EDLCs in different electrolytes within 0-2.4 V at 0.5 A g^{-1}. (b) Cyclic voltammetry curves of the EDLCs in different electrolytes within 0-2.4 V at 10 mV s^{-1}. (c) Rate capability of EDLCs in different electrolytes with current densities increasing from 0.5 to 10 A g^{-1}. (d) Cyclic voltammetry curves of various electrolytes within 0-2.4 V at 100 mV s^{-1}. (e) Nyquist curves of the

EDLCs with different electrolytes and (f) plots of imaginary specific capacitance versus frequency in different electrolytes. (g) Cycle stability of EDLCs in 3 m hybrid electrolyte within 0-2.4 V at 8 A g^{-1} and (h) the charge-discharge curves of EDLCs in 3 m hybrid electrolyte at specific cycles.

Besides the operating voltages, the rate capability is another key consideration for EDLCs. As shown in Figure 2c and S5 (supporting information), the EDLCs in the 3 m hybrid electrolyte demonstrates the best rate capability, which maintained 69% of the initial capacitance (measured at 0.5 A g^{-1}) even when the current density is increased to 10 A g^{-1} (enabling a full discharge in 9 s). By contrast, the EDLCs with the 1 m $NaClO_4$ in TMP electrolyte merely provide 11% initial capacitance at the same condition. Moreover, the superior rate capability of the EDLCs with the 3 m hybrid electrolyte is also verified by the cyclic voltammetry curves which featured the largest integration area and the least distortion at different scan rates (Figure 2d and S6, supporting information). In accordance with cyclic voltammetry tests, the electrochemical impedance spectra (EIS) (Fig. 2e and 2f) show that the EDLCs in the 3 m hybrid electrolyte exhibit the smallest charge transfer resistance and the shortest relaxation time constant (τ_0), indicating the most efficient ion transportation.[12] Besides, we further studied the ionic conductivity and viscosity of the hybrid electrolytes, and the 3 m hybrid electrolyte show medium ionic conductivity and viscosity (Figure S7, supporting information). Based on these results, the 3 m hybrid electrolyte is the optimal electrolyte in a balanced view of both electrochemical window and rate capability.

The cycle stability of the EDLCs with the 3 m hybrid electrolyte was further investigated by galvanostatic charge-discharge technique at 8 A g^{-1} within the voltage range of 0-2.4 V. A capacitance retention of 83% is achieved after 100, 000 cycles at 8 A g^{-1} (Figure 2g and 2h), verifying an excellent long-term cycle stability of the 3 m hybrid electrolyte within the voltage range of 0-2.4 V. Even after 100, 000 cycles, only small increases in the charge

transfer resistance and τ_0 of the EDLCs are observed, further indicating the stability of the EDLCs in the hybrid electrolyte (Figure S8a, supporting information). These observations are also supported by the analysis of the morphology and elemental composition of the aMEGO electrodes by SEM and energy dispersive X-ray (EDX) spectroscopy (Figure S9, supporting information) after 100, 000 cycles where no resultants of electrolyte decomposition were detected. Moreover, the plots of the real specific capacitance versus frequency (Figure S8b, supporting information) show a capacitance retention of 91% after 100, 000 cycles at 10 mHz.

A wide operating temperature range is a necessary for the practical application of EDLCs with aqueous-based electrolytes. In this work, the electrochemical performance of the EDLCs with the 3 m hybrid electrolyte was evaluated under different temperatures ranging from -20°C to 60°C. While the specific capacitance of the EDLCs is higher at 60℃ (e.g., 120 Fg^{-1} at 3 A g^{-1}), 70% of the specific capacitance is still maintained when the temperature is decreased from 60 to -20°C (Figure 3a). Meanwhile, the rate capabilities of the EDLCs are similar regardless of operating temperatures. The galvanostatic charge-discharge curves of the EDLCs with the 3 m hybrid electrolyte retain linear and symmetric in the wide temperature range from -20 °C to 60 °C (Figure 3d-3f). When the current density is increased from 1 to 3 A g^{-1}, 86% (from 96 to 83 F g^{-1}), 90% (from 108 to 98 F g^{-1}), and 88% (from 137 to 120 F g^{-1}) of the specific capacitance can still be obtained at -20°C, 0°C, and 60°C, respectively. Moreover, the EIS results reveal a small change in charge transfer resistance and τ_0 with changing temperatures (Figure 3b and 3c), indicating the wide temperature compatibility of the 3 m hybrid electrolyte and its decent capability for charge transfer even at the reduced temperatures.

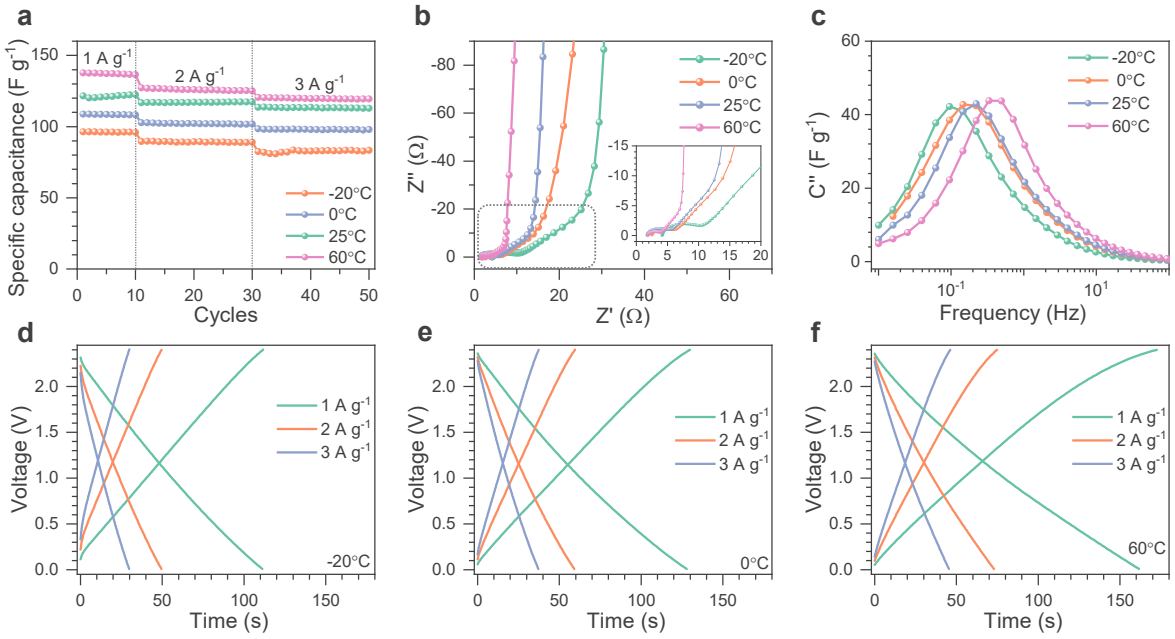

Figure 3. Electrochemical performance of aMEGO-based EDLCs with 3 m hybrid electrolyte at different temperatures ranging from -20 to 60°C. (a) The specific capacitance calculated from galvanostatic charge-discharge curves at different temperatures and current densities. (b) The Nyquist curves at different temperatures, inset is the enlarged image of the region marked by grey dashed rectangular. (c) The plots of the imaginary specific capacitance *vs*. frequency at different temperatures. The galvanostatic charge-discharge curves at different current densities at (d) -20 °C, (e) 0 °C, and (f) 60 °C.

To explore the origin of the extended electrochemical window and the wide temperature compatibility of the 3 m hybrid electrolyte, Raman spectroscopy was performed to investigate the interaction between electrolyte ions and solvent molecules in different electrolytes, *i.e.*, pure water, TMP solvents, and the hybrid electrolytes, as presented in Figure S10 (Supporting Information). For the Raman shift from 700 to 800 cm^{-1} (Figure S10a), two broad peaks centered at 737 and 752 cm^{-1} are observed in all samples containing TMP, which are ascribed to the stretching vibration of P-O-C groups from isolated TMP molecules.[13] For the Raman shift from 2700 to 4200 cm^{-1} (Figure S10b), the broad peak observed in pure water and the 1 m $NaClO_4$ aqueous electrolyte can be devolved into four bands, *i.e.*, the

bands at 3230 and 3420 cm^{-1} corresponding to the four-hydrogen bonded water molecules (free water), and the bands at 3540 and 3610 cm^{-1} corresponding to the partially hydrogen bonded water molecules (non-free water). [14] In sharp contrast, the intensity of the bands of four-hydrogen bonded water molecules in the 18 m $NaClO_4$ aqueous electrolyte is much lower than that in the pure water and the dilute 1 m $NaClO_4$ aqueous electrolyte. For the hybrid electrolytes, only the bands corresponding to the partially hydrogen bonded water molecules are observed, indicating that the water molecules are solvated.

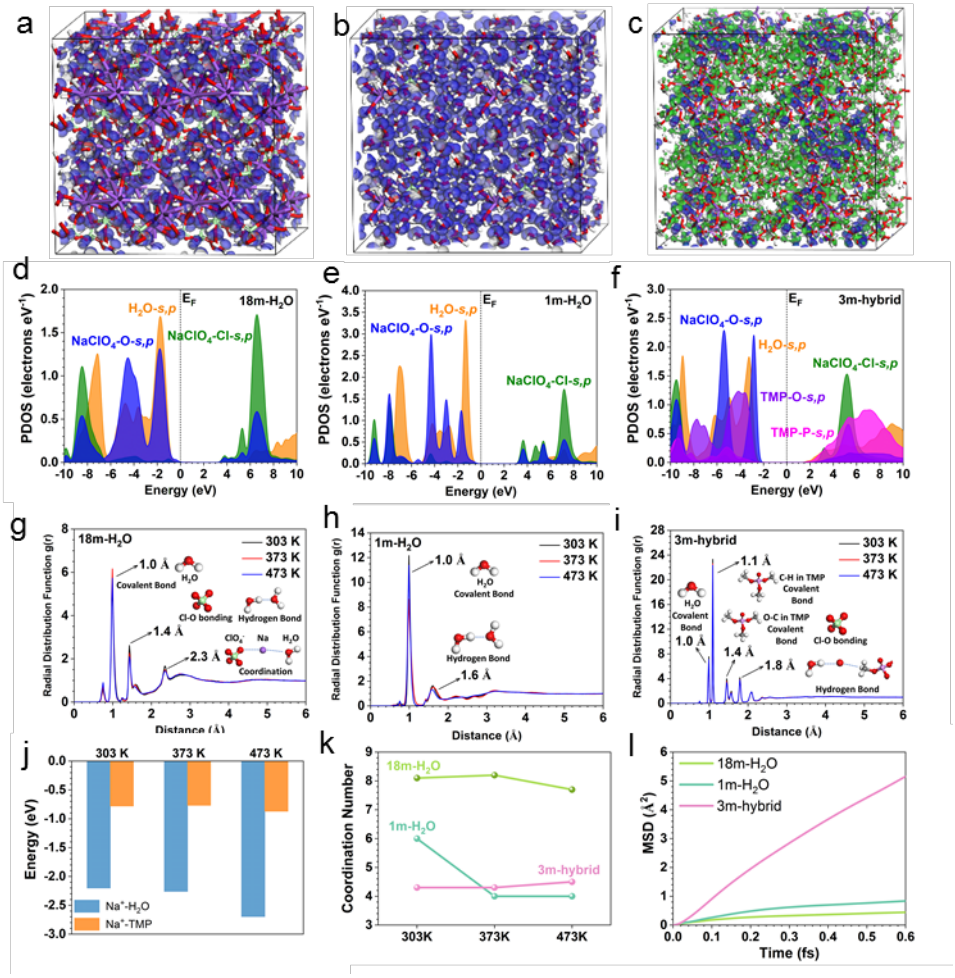

Figure 4. The 3D contour plot of the anti-bonding and bonding orbitals of (a) the 18 m $NaClO_4$ aqueous electrolyte, (b) 1 m $NaClO_4$ aqueous electrolyte, and (c) 3 m hybrid electrolyte. Red= O, white= H, purple = Na, light green = Cl, pink = P. The PDOS of (d) 18 m $NaClO_4$ aqueous electrolyte, (e) 1 m $NaClO_4$ aqueous electrolyte, and (f) 3 m hybrid electrolyte. The RDF comparison of (g) 18 m $NaClO_4$ aqueous electrolyte, (h) 1 m $NaClO_4$ aqueous electrolyte, and (i) 1 m $NaClO_4$ aqueous electrolyte. (j) The binding

energies comparison of Na^+-H_2O and Na^+-TMP at 303 K, 373 K, and 473 K. (k) The coordination numbers of Na in different electrolytes at 303 K, 373 K, and 473 K. (l) The mean square displacement of different electrolytes at 303 K.

Moreover, the molecular dynamic (MD) simulations were employed to depict the solvation structures in different electrolytes including the 3 m $NaClO_4$ hybrid electrolyte, 1 m dilute and 18 m super-concentrated aqueous $NaClO_4$ electrolytes. For the 18 m super-concentrated (Figure 4a) and 1 m dilute $NaClO_4$ aqueous electrolytes (Figure 4b), the electronic density mainly locates in the water molecules, indicating the preference of water molecules with Na^+ cations. With the introduction of TMP into the electrolyte, the bonding orbitals still locates on the water molecules, while the anti-bonding orbitals locate on the TMP molecules (Figure 4c). This indicates that the Na ions prefer the bonding with electron-rich water molecules while the introduced TMP are able to freely migrates in the electrolyte solution.

The detailed electronic structures are further revealed by the projected partial density of states (PDOS). Notably, in the 18 m $NaClO_4$ aqueous electrolyte, the *s,p* orbitals of both ClO_4^- anions and water molecules demonstrate the well-overlapped features, supporting their strong interactions (Figure 4d). For the 1 m $NaClO_4$ aqueous electrolyte, a closer position to the Fermi level (E_F) of the *s, p* orbitals of the water molecules is observed, indicating that the bonding of water molecule becomes dominant in the electrolyte (Figure 4e). For the 3 m hybrid electrolyte (Figure 4f), the TMP molecules result in a significant band offset of valence and conduction bands. However, both ClO_4^- and H_2O still dominate the valence band maximum (VBM) with the preferred bonding trending of Na^+ ions. Although the *s,p* orbitals of TMP-O locate at a deeper position, the *s,p* orbitals of TMP-P has significantly modified the conduction band minimum (CBM), supporting the freely migration of the TMP molecules

in the electrolyte solution.

The radial distribution function (RDF) of these electrolytes after the MD simulations at different temperatures has been demonstrated (Figure 4g, 4h and 4i). And the results depict that temperature does not impose strong effects on the bonding of the electrolyte solution. In the 18 m $NaClO_4$ aqueous electrolyte, the main bonding is the O-H in water molecules with a sharp peak at 1.0 Å. The second obvious peak at 1.4 Å is attributed to the Cl-O in ClO_4^- and the hydrogen bonding in the solution. In addition, another peak of 2.3 Å represents the coordinated environment of Na ions by both ClO_4^- and water (Figure 4g). In contrast, the 1 m $NaClO_4$ aqueous electrolyte only shows two evident peaks at 1.0 Å and 1.6 Å, which are assigned to the O-H bonding in water molecules and the hydrogen bonding, respectively. Due to the dilute concentration, the coordination bonding of Na ions only exhibits very weak peaks near 2.3 Å in the RDF results (Figure 4h). After the introduction of TMP, the bonding environment of the electrolyte has been evidently modified with more peaks in the RDF results under different temperatures. For the 3 m hybrid electrolyte, instead of the O-H bonding in water molecules, the C-H bonding with a length of 1.1 Å in TMP becomes the dominant peak in RDF results. Meanwhile, both O-C and O-Cl bonding in TMP and ClO_4^- contribute to the peak at 1.4 Å. The subtle peak at 1.6 Å denotes the P-O bonding in TMP. With the introduced TMP, more possible hydrogen bonding leads to a peak at 1.8 Å. These results interpreted that the TMP does not show strong interaction with Na^+ ions (Figure 4i).

Then, we further compare the binding energies between Na^+-H_2O and Na^+-TMP, in which Na^+-H_2O shows much stronger binding strength than the Na^+-TMP from 303 K to 473 K. This indicate that the water has been constrained near Na^+ ions to form the stable solvation shell while the TMP can freely migrate to enable the wider voltage window for the EDLCs (Figure 4j). For the coordination number (CN) change of Na^+ ions, we notice that TMP not only alleviates the decreasing trend of CN as temperature increase but also slightly increases

the CN. Compared to the pure aqueous electrolytes, hybrid electrolyte lowers the CN due to isolation by the TMP with weak bonding with Na^+ ions in the electrolyte (Figure 4k). The mean square displacement (MSD) support that a much higher diffusion of molecules in hybrid electrolyte induced by the migrating TMP, supporting the hybrid electrolyte significantly promotes the charge-discharge efficiency of the EDLCs (Figure 4l).

Conclusion

In summary, we introduced the TMP to regulate the solvation structure in hybrid electrolytes with low concentrations, achieving a comparable electrochemical window to super-concentrated aqueous electrolytes. DFT calculations have confirmed that the water molecules are strongly coordinated to Na cations to form a primary solvation shell which is isolated by the freely migrated TMP molecules due to the binding energy difference. In such solvation structure, the water activity is largely restrained in the hybrid electrolyte. Meanwhile, the TMP not only decreases the solvation shell of Na cations in the hybrid electrolyte but also increases the diffusion efficiency. By optimizing the composition of hybrid electrolytes, the 3 m hybrid electrolyte reaches an optimal balance among the electrochemical window (3.0 V), ionic conductivity (23 mS cm^{-1}), density (1.37 g cm^{-3}), and temperature compatibility (-20-60 ºC). As a result, the EDLCs with the hybrid electrolyte can operate at a high voltage up to 2.4 V and a broad temperature range as well as deliver excellent rate capability and cycle stability. Based on the insight solvation mechanism of dilute hybrid electrolytes, our work suggests that introducing aprotic solvent in aqueous electrolytes is an effective and promising approach to tailor the solvation structure and achieve the low-cost EDLCs with high operation voltage, excellent rate capacity, and wide temperature compatibility. This work will significantly benefit the future research in

optimizing the electrolyte properties for more applications of energy conversion.

Acknowledgements

We are grateful for financial support from the General Research Fund (GRF CityU 1307619), CityU Applied Research Grant (ARG 9667208), and the National Science Foundation of China (51872249).

Reference:

[1] D. L. Chao, S. Z. Qiao, *Joule* **2020**, *4*, 1846-1851.

[2] P. Simon, Y. Gogotsi, *Nature Materials* **2008**, *7*, 845-854.

[3] F. Beguin, V. Presser, A. Balducci, E. Frackowiak, *Adv Mater* **2014**, *26*, 2219-2251.

[4] C. Zhong, Y. D. Deng, W. B. Hu, J. L. Qiao, L. Zhang, J. J. Zhang, *Chem Soc Rev* **2015**, *44*, 7484-7539.

[5] a) W. J. Qian, J. Texter, F. Yan, *Chem Soc Rev* **2017**, *46*, 1124-1159; b) D. W. Xiao, Q. Y. Dou, L. Zhang, Y. L. Ma, S. Q. Shi, S. L. Lei, H. Y. Yu, X. B. Yan, *Adv Funct Mater* **2019**, *29*.

[6] L. Smith, B. Dunn, *Science* **2015**, *350*, 918-918.

[7] a) L. M. Suo, O. Borodin, T. Gao, M. Olguin, J. Ho, X. L. Fan, C. Luo, C. S. Wang, K. Xu, *Science* **2015**, *350*, 938-943; b) L. M. Suo, O. Borodin, Y. S. Wang, X. H. Rong, W. Sun, X. L. Fan, S. Y. Xu, M. A. Schroeder, A. V. Cresce, F. Wang, C. Y. Yang, Y. S. Hu, K. Xu, C. S. Wang, *Adv Energy Mater* **2017**, *7*, 1701189; c) L. W. Jiang, Y. X. Lu, C. L. Zhao, L. L. Liu, J. N. Zhang, Q. Q. Zhang, X. Shen, J. M. Zhao, X. Q. Yu, H. Li, X. J. Huang, L. Q. Chen, Y. S. Hu, *Nat Energy* **2019**, *4*, 495-503; d) L. M. Suo, O. Borodin, W. Sun, X. L. Fan, C. Y. Yang, F. Wang, T. Gao, Z. H. Ma, M. Schroeder, A. von Cresce, S. M. Russell, M. Armand, A. Angell, K. Xu, C. S. Wang, *Angew Chem Int Edit* **2016**, *55*, 7136-7141; e) Y. Yamada, K. Usui, K. Sodeyama, S. Ko, Y. Tateyama, A. Yamada, *Nat Energy* **2016**, *1*, 16129; f) S. Ko, Y. Yamada, K. Miyazaki, T. Shimada, E. Watanabe, Y. Tateyama, T. Kamiya, T. Honda, J. Akikusa, A. Yamadaa, *Electrochem Commun* **2019**, *104*, 106488; g) L. W. Jiang, L. L. Liu, J. M. Yue, Q. Q.

Zhang, A. X. Zhou, O. Borodin, L. M. Suo, H. Li, L. Q. Chen, K. Xu, Y. S. Hu, *Adv Mater* **2020**, *32*, 10, 1904427.

[8] a) X. D. Bu, L. J. Su, Q. Y. Dou, S. L. Lei, X. B. Yan, *J Mater Chem A* **2019**, *7*, 7541-7547; b) M. R. Lukatskaya, J. I. Feldblyum, D. G. Mackanic, F. Lissel, D. L. Michels, Y. Cui, Z. A. Bao, *Energ Environ Sci* **2018**, *11*, 2876-2883.

[9] a) H. B. Bi, X. S. Wang, H. L. Liu, Y. L. He, W. J. Wang, W. J. Deng, X. L. Ma, Y. S. Wang, W. Rao, Y. Q. Chai, H. Ma, R. Li, J. T. Chen, Y. P. Wang, M. Q. Xue, *Adv Mater* **2020**, *32*, 2000074; b) Z. G. Hou, M. F. Dong, Y. L. Xiong, X. Q. Zhang, Y. C. Zhu, Y. T. Qian, *Adv Energy Mater* **2020**, *10*, 10, 1903665.

[10] P. Lannelongue, R. Bouchal, E. Mourad, C. Bodin, M. Olarte, S. le Vot, F. Favier, O. Fontaine, *Journal of the Electrochemical Society* **2018**, *165*, A657-A663.

[11] J. Xie, Z. Liang, Y.-C. Lu, *Nature Materials* **2020**, *19*, 1006-1011.

[12] F. Y. Chi, C. Li, Q. Q. Zhou, M. Zhang, J. Chen, X. W. Yu, G. Q. Shi, *Adv Energy Mater* **2017**, *7*.

[13] a) H. Nakagawa, M. Ochida, Y. Domi, T. Doi, S. Tsubouchi, T. Yamanaka, T. Abe, Z. Ogumi, *J Power Sources* **2012**, *212*, 148-153; b) P. C. Shi, H. Zheng, X. Liang, Y. Sun, S. Cheng, C. H. Chen, H. F. Xiang, *Chem Commun* **2018**, *54*, 4453-4456.

[14] a) Y. H. Zhang, C. K. Chan, *Journal of Physical Chemistry A* **2003**, *107*, 5956-5962; b) G. E. Walrafen, *Journal of Chemical Physics* **1970**, *52*, 4176-+; c) D. M. Carey, G. M. Korenowski, *Journal of Chemical Physics* **1998**, *108*, 2669-2675.